PHYSICAL REVIEW B VOLUME 18, NUMBER 5 1 SEPTEMBER 1978

Third sound, two-dimensional hydrodynamics, and elementary excitations in very thin helium films*

J. E. Rutledge, W. L. McMillan, and J. M. Mochel
Physics Department and Materials Research Laboratory, University of Illinois, Urbana, Illinois 61801

T. E. Washburn
Watkins Johnson Company, Stanford Industrial Park, Palo Alto, California 94302

(Received 24 February 1977)

High-precision measurements of third-sound velocity in ^{4}He films with surface densities between 0.16 and 5.25 atomic layers have been taken between 0.1 and 1.5 K. By reformulating Landau's quantum hydrodynamics in two dimensions we have been able to accurately describe these measurements in terms of a surface phonon and surface roton branch of the elementary excitation spectrum. In the thin-film limit surface tension falls to zero and the surface rotons are characterized by an energy gap of 5.3 K.

I. INTRODUCTION

We present high-precision measurements of third-sound velocity in ^{4}He films between 0.1 and 1.5 K for superfluid surface densities between 0.16 atomic layers and 5.25 atomic layers. We argue that the film thickness and the healing length are not definable for monolayer films and we provide a workable theory by reformulating Landau's quantum hydrodynamics using only the areal density. The theory predicts the surface-phonon branch of the elementary excitation spectrum and we add the surface-roton branch in an *ad hoc* way. We then can calculate the temperature dependence of the third-sound velocity from the elementary excitation spectrum. Finally, we fit the measured third-sound velocity by adjusting parameters in the elementary excitation spectrum. In this way we find an experimental elementary excitation spectrum with a surface-phonon branch with upward dispersion due to surface tension and consistent with a surface-roton branch with a gap of about 5.3 K at shorter wavelength.

Third-sound waves in thick ^{4}He films were first generated and detected using a chopped infrared beam and a polarimeter by Everitt *et al.*[1] in 1962. Third-sound waves are similar to shallow-water waves. However, Atkins[2] pointed out two modifications necessary to describe their behavior in thick helium films. First, the restoring force is not gravity by the Van der Waals force $F(D)$ binding the helium atoms to the substrate. $F(D)$ varies as D^{-4} for thick films where D is the film thickness. A detailed measurement of $F(D)$ on CaF$_2$ has been performed by Anderson and Sabisky.[3] Second, only the superfluid fraction ρ_s/ρ of the liquid portion d can participate in the wave motion. The remaining thickness $(D-d)$ is primarily the solidified layer of helium on the substrate. The resulting expression for surface-wave phase velocity

$$c_s^2 = \left[F(D)\frac{\rho_s}{\rho}D + \frac{k^2\beta D}{\rho}\right]\frac{\tanh(kD)}{kD} \tag{1}$$

contains two terms. The first term dominates for $kd \ll 1$, where k is the wave vector, and gives the third-sound velocity. For $kd \gg 1$, the second term, proportional to the surface tension β, dominates. The surface wave goes over to the bulk-surface wave, the deep-water wave, and these elementary excitations are called ripplons.[4]

Third sound became a tool to understand thin helium films with the work of Kagiwada *et al.*[5] Time-of-flight measurements of third-sound velocity were made with a pulsed resistive heater and an aluminum superconducting bolometer. Additional measurements at constant thickness down to coverages of 2.1 atomic layers and temperatures of 0.1 K by Scholtz *et al.*[6] provided third-sound velocities with a precision of 1 part in 10^3. They interpreted their measurements within the framework of the Ginzburg-Pitaevskii (GP) theory[7] to produce a temperature-dependent healing length. This healing length describes the variation of the superfluid density perpendicular to the substrate. Near T_c, where the healing length is macroscopic, and for thick films the GP theory should be valid; however there are still unresolved questions about the boundary conditions. For thin films with a superfluid surface density of order one atomic layer the GP healing length concept is clearly not applicable at any temperature. Even the film thickness D is a fuzzy concept and is definable only with an accuracy of monolayer. For monolayer superfluid films the film thickness is not a macroscopically definable quantity and it cannot be used in the macroscopic hydrodynamic theory to derive Eq. (1). Figure 1 illustrates schematically these difficulties. The outermost atoms in this figure should be drawn blurred in the horizontal direction by at least a free-particle de Broglie wavelength λ_F.

By allowing the helium film to close upon itself on the inner surface of a quartz capsule, we have been able to establish a third-sound resonance. As a result we have been able to measure the third sound velocity to 1 part in 10^5. The observed T^3 dependence[8] of the changes in the square of the third-sound velocity at low temperatures suggested a two-dimensional spectrum of Landau elementary excitations (surface phonons). The thermally excited elementary excitations form a normal fraction which is pinned to the substrate; the resulting reduction in the superfluid surface density explains the T^3 dependence of $c_3^2(T)$. This point of view is common to bulk ^{4}He where, below 1 K, Landau's elementary excitations[9] describe the normal fraction. This interpretation, for restricted geometries, is also argued for by Padmore and Reppy.[10]

Padmore[11] has calculated the elementary excitation spectrum of a strictly two-dimensional ^{4}He system using the Feynman-Cohen method. He finds a surface roton with a gap less than the bulk roton gap for areal densities less than one atomic layer. Chester[12] has pointed out that the order of magnitude and temperature dependence of Scholtz's data above 0.8 K can be explained by a surface-roton contribution to the normal surface density. Thus the surface phonon and surface roton have been discussed previously.

We have carried out an extensive set of measurements of third-sound velocity on thin films. In order to understand our measurements we have developed the natural macroscopic theory for thin films, an extension of Landau's quantum hydrodynamics. We assume a two-dimensional condensate wave function $\psi(\vec{x})$ from which we can generate a two-dimensional superfluid hydrodynamics. The elementary excitations appear as collective modes of the condensate. The thermodynamic calculations are then standard. The concept of superfluidity in a two-dimensional system is an interesting one; we should emphasize that our films are thin enough to be truly two dimensional. Hohenberg has shown that there is no long-range order at finite temperature in a two-dimensional superfluid. However, at low temperature the superfluid correlations extend over great distances which can be greater than the wavelength of our third-sound probe ($\sim$1 cm). One would then expect to observe superfluid behavior and we do observe a third sound mode with a mean free path greater than 10^4 cm (cavity $Q \sim 10^4$). The question of superfluidity is a subtle one and involves a discussion of dissipative mechanisms. We will present a detailed study of third-sound dissipation in a separate paper. For our present purposes it is sufficient to note that one can define a condensate wave function in the ground state (at zero temperature) in two dimensions and this is all that is required for quantum hydrodynamics. Our theoretical model predicts the correct correlation function at finite temperature.

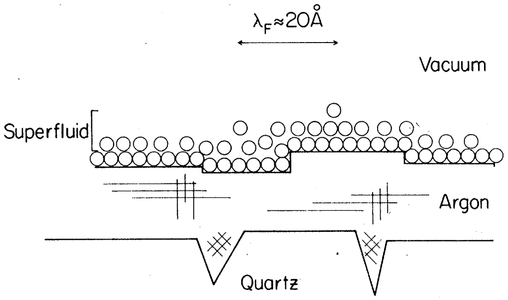

FIG. 1. Schematic of the substrate and adsorbed helium film. This sketch might correspond to a coverage of 1.5 atomic layers. The outer layer should be blurred in the horizontal direction by at least the free-particle de Broglie wavelength.

The helium films we have studied were absorbed on an estimated 15 atomic layers of argon. We assume that down to a helium coverage of 1.2 atomic layers the interaction with the argon substrate is dominated by the standard Van der Waals $1/D^3$ interaction. Down to a coverage of 2.75 atomic layers on argon the measurements of Anderson and Sabisky clearly establish the helium-substrate interaction to be $1/D^3$. There is no thermodynamic data for helium coverages less than 2.75 atomic layers on a weak binding substrate—that is, for first layer binding energies characterized by a Γ of less than 50 K. However, there is indirect evidence from third-sound studies that the standard Van der Waals attraction of $1/D^3$ dominates for smaller coverages. Scholtz *et al.*[6] demonstrate this dominance down to 2 atomic layers on glass and CaF$_2$. More recently, Berthold, Bishop and Reppy[13] successfully interpreted third-sound velocity measurements down to 0.06 atomic layers of *mobile helium* by assuming only a Van der Waals interaction. Finally, it is interesting to note that the 4.2-K isotherm data of Lerner and Daunt[14] for ^{4}He absorbed on grafoil preplated with a monolayer of argon can be fit to within 5% of coverage down to 1.2 atomic layers of ^{4}He by the Frenkl-Halsey-Hill isotherm with a Γ of 60 K. This Γ can also be obtained by using a $1/D^3$ model for the compositie surface. Thus, in this paper, we will assume a $1/D^3$ interaction even for our thinnest films. This assumption establishes the form of the Hamiltonian in Sec. III and is verified by the agreement between the calculated and measured third sound velocity at $T=0$.

The plan of the paper is as follows: In Sec. II we discuss the experiment and present the working data in Table I. We develop, in Sec. III, the two-dimensional quantum hydrodynamics bringing in a parameter B, related to surface tension, a two-dimensional "rotonlike" excitation, and an extension to slightly thicker films. From this model an expression for the third-sound velocity at finite temperature is derived. In Sec. IV the analysis of the experimental results, within the above framework is described. The results and conclusions are presented in Sec. V and in Table II.

II. EXPERIMENT

We have measured the temperature dependence of the third-sound velocity $c(T)$, the vapor pressure over the helium film $P(T)$, and determined the total area density $D(T)$ in units of atomic layers (1 atomic layer is 7.7×10^{14} atoms/cm^2) from the vapor-pressure curve using the Frenkel-Halsey-Hill isotherm equation. Here we describe the measurements and the data analysis.

A. Cell

The helium film lies on an argon substrate inside of a $0.7\times2\times0.001$-cm quartz envelope, called a cell, constructed from two thin (0.002–0.004-in.) optically flat sheets of vitreous quartz. First a hole having about a 0.004-in. diameter to serve as an electrical feed-through and a means of admitting the argon is made in each of the quartz sheets. The hole is burned through each sheet by focusing a $\frac{1}{20}$-sec pulse from a CO_2 laser operating at about 3 W total power. The resulting holes are smooth and the quartz sheet around each hole us not thickened or distorted. On one side we evaporate a 4×10-mm rectangular aluminum capacitor plate 2000 Å thick with the hole included in the area of the plate. On the other side an 8000-Å-thick aluminum dot is evaporated over the hole. During the evaporation, enough aluminum condenses into the hole from each side to form a continuous film and provide eelectrical contact between the dot and the capacitor plate, which will eventually be on the inner wall of the cell. Finally 3000 Å of silicon monoxide are evaporated over one of the aluminum plates to prevent the two plates from shorting together.

The quartz sheets are then pressed between two stainless steel rectangular anvils with the aluminum capacitor plates face to face. The faces of the anvils have a length and width 3 mm smaller than those of the sheets so that the edges of the sheets extend beyond the anvils by $1\frac{1}{2}$ mm on all sides. In addition the top anvil is hollowed out to within $\frac{1}{32}$ in. of its bottom and filled with tin. After placing the sheets between the anvils, their edges are melted together with a small oxy-hydrogen torch. While welding the edges, care is taken so that the tin does not melt, guaranteeing that the aluminum films are kept cool enough to avoid bubbling. The result is a cell with about 0.001 cm inside separation and two capacitor plates separated by this distance.

Finally, a heater and thermometer are attached and the cell is filled with argon gas. The heater is made by evaporating a $\frac{1}{10}$-in.-wide Chromel A strip at one end of the cell and across its width. During the evaporation, the heater's resistance is monitored and the evaporation is stopped when the resistance reaches 1000 Ω. At the opposite end of the cell, a $\frac{1}{10}$-in-wide DAG paint[15] carbon-resistance thermometer is painted across the width of the cell. Finally, the holes through the cell are plugged with epoxy while the cell is filled with and surrounded by $\frac{5}{6}$ atm of argon gas. When the cell is cooled, a thick argon film solidifies from the vapor phase on the inside walls of the cell to form the substrate for the film. See Fig. 2.

The end of the cell is then glued with a small amount of Epoxy to a heat sink and mounted inside a brass can attached to the mixing chamber of a dilution refrigerator. The helium required to form the film is put into the cell by diffusing it through the quartz walls. To fill the cell, the brass can is filled with an appropriate pressure helium gas while the can and cell are at room temperature. The helium diffuses to equilibrium in 24 h and after this period of time the cell and refrigerator are cooled to 77 K. The can is then evacuated to 10^{-6} Torr before cooling into the experimental temperature range.

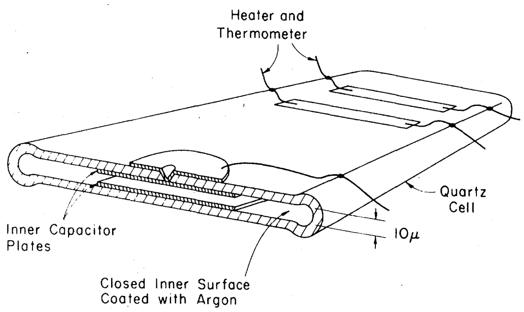

FIG. 2. Schematic of the quartz cell. A thin-film heater on the outside of the cell excites third sound in the superfluid ^{4}He film on the inner surface. The thermometer at the opposite end of the cell detects the temperature oscillations due to third-sound resonance. The capacitor plates allow *in situ* pressure measurements for a determination of film thickness.

B. Temperature scale

The temperature scale is established below 4 K by a Superconducting Fixed Point Thermometer[16] purchased from the National Bureau of Standards (NBS). The fixed points are used to calibrate a noise thermometer which is in turn used to calibrate the carbon resistors, including the DAG thermometer on the cell, that are used as working thermometers during the experimental run. Below 4 K our temperature scale is accurate to 1.5%.

Above 4 K our temperature scale is provided by a commercial germanium resistance thermometer[17] measured at 22 Hz with a low-noise ac resistance bridge.[18]

C. Third-sound velocity

As the cell cools below about 10 K, the helium condenses on the already frozen argon and forms a continuous film on the inside the cell. Below 1 K, third-sound waves can be generated and detected. As the heater drives temperature oscillations in the adjacent quartz wall, third-sound waves radiate over the film. Because the film covers the entire inside surface of the cell, it is possible to set up a third-sound resonance if, for a given path on the inside surface of the cell, the third-sound wave can return to the heater with its temperature oscillations in phase with the heater. The lowest-frequency resonance the cell can sustain corresponds to having a third-sound wave travel the length of one sheet down to the thermometer and return to the heater up the length of the other sheet. The temperature oscillations are much larger (in fact by as much as 10^4 times larger) for the standing-wave resonance modes than for the nonresonant signals. It is this that allows the high resolution we achieve for c_3, the third-sound velocity. We obtain the third-sound velocity by multiplying the frequency at which the lowest standing-wave mode is observed by the inside perimeter of the cell.

In practice even at resonance, the temperature oscillations of the thermometer are quite small (10^{-10} K) at the lowest temperatures and for the thinnest films. To detect the temperature oscillations of the thermometer a constant current is passed through it and the resulting voltage oscillations due to $(\partial R/\partial T)\Delta T$ are then measured with a lock-in amplifier. The heater frequency is swept through a narrow range ($\Delta f/f \approx 10^{-3}$) so that the entire lineshape of the third-sound resonance is measured. The amplified and demodulated signal from the lock-in amplifier is averaged (5 min to 10 h) until the signal-to-noise ratio is sufficient to determine the resonant frequency to about $\frac{1}{5}$ of the full width at half-maximum (FWHM). Near the transition temperature the ratio of the resonant frequency to the FWHM is about 10, but the ratio grows rapidly to as large as 2×10^4 as the cell is cooled. This establishes the high resolution of our velocity measurement.

D. Film thickness

The aluminum films on the inside walls of the cell form a parallel plate capacitor. As the temperature of the cell rises above 0.6 K the film begins to evaporate and the rising pressure causes the cell walls to move apart and the capacitance decreases. The distance between the walls is governed by Hooke's law

$$P = K(x - x_0) \ ,$$

where P is the pressure, x is the spacing between the plates, and x_0 is the $P=0$ spacing. This is verified by applying external gas pressure at 4.2 K and measuring the capacitance. The spring constant k does not change as a function of temperature over the range of interest as determined by measuring the vapor pressure of bulk ^{3}He in the cell at the Cd fixed point of the NBS standard and comparing the result to the ^{3}He vapor-pressure tables. The spring constant k measured at 30 K is also identical to the one at 4.2 K as determined by external gas-pressure measurement.

The coverage is determined from the Frenkel-Halsey-Hill isotherm at low temperatures

$$\ln(P_0/P) = A/TD^3 \ ,$$

where P_0 is the bulk vapor pressure and A is 14.5 K. We cannot directly measure the isotherm because we cannot independently determine the total amount of helium in the cell. We determine D by measuring P as a function of T and fitting the isotherm equation to obtain D vs T. Since the capacitance C is proportional to $1/d$ we have

$$P = k'(C - C_0)/C \ .$$

Our measurements have a sensitivity to pressure of about 10^{-4} Torr.

The experimental data for 11 different surface densities are presented in Table I. $c_{3e}(T)$ is calculated from the resonant frequency as described in this section with the cell perimeter taken to be 3.82 cm. $c_{3T}(T)$ are the velocities resulting from the theory of Sec. III and the fitting procedure described in Sec. IV.

III. THEORY

A. Quantum hydrodynamics

We propose a theoretical model for superfluidity in thin helium films. We assume that a condensate wave function exists and write down a phenomenological equation of motion for the macroscopic superfluid

TABLE I. T, $c_{3e}(T)$, and $D(T)$ are from measurement. Temperature T is known to ±1.5% or ±5 mK. $D(T)$, the coverage of ^{4}He, is calculated from *in situ* pressure measurements with an absolute uncertainty of 5%. $c_{3e}(T)$ is calculated from the resonant frequency, which at low temperatures is measured to two parts in 10^5, and the internal circumference of the cells, 3.82 cm. $c_{3T}(T)$ is calculated using the model described here.

Run	T (K)	$c_{3e}(T)$ (cm/sec)	$D(T)$ (atomic layers)	$c_{3T}(T)$ (cm/sec)
I	0.100	6335.50	1.41	6334.41
	0.150	6325.30	1.41	6321.75
	0.150	6328.10	1.41	6321.75
	0.200	6307.60	1.41	6297.79
	0.250	6204.60	1.41	6255.54
	0.300	6158.30	1.41	6180.53
	0.350	6075.30	1.41	6053.03
	0.375	6098.00	1.41	5963.30
	0.400	5931.50	1.41	5853.22
	0.425	5913.30	1.41	5720.62
	0.450	5593.00	1.41	5563.47
II	0.112	6279.10	1.45	6275.83
	0.153	6267.70	1.45	6267.75
	0.187	6257.10	1.45	6257.22
	0.260	6219.80	1.45	6218.94
	0.300	6183.40	1.45	6183.20
	0.332	6136.20	1.45	6141.06
	0.342	6120.30	1.45	6124.48
	0.406	5975.10	1.45	5963.02
	0.424	5899.90	1.45	5895.23
	0.449	5754.70	1.45	5780.14
	0.466	5507.70	1.45	5686.11
III	0.147	6805.10	1.77	6804.23
	0.191	6801.00	1.77	6801.07
	0.224	6797.50	1.77	6797.75
	0.252	6794.30	1.77	6794.21
	0.282	6789.80	1.77	6789.56
	0.319	6782.50	1.77	6782.29
	0.341	6777.90	1.77	6776.95
	0.355	6773.10	1.77	6773.05
	0.374	6767.10	1.77	6767.05
	0.393	6759.90	1.77	6760.11
	0.411	6752.70	1.77	6752.57
	0.428	6743.20	1.77	6744.46
	0.445	6734.20	1.77	6735.32
	0.465	6723.00	1.77	6723.11
	0.482	6711.80	1.77	6711.41
	0.500	6696.50	1.77	6697.60
	0.518	6681.20	1.77	6682.25
	0.544	6657.40	1.77	6657.20
	0.570	6629.10	1.77	6628.61
	0.599	6595.30	1.77	6592.33
	0.623	6559.60	1.77	6558.72
	0.651	6514.30	1.77	6515.33
	0.681	6453.90	1.77	6463.73
IV	0.132	6619.60	1.85	6620.22
	0.162	6618.70	1.85	6618.89
	0.204	6616.30	1.85	6616.30
	0.250	6612.80	1.85	6612.44
	0.298	6607.70	1.85	6607.20
	0.348	6600.40	1.85	6600.31
	0.405	6590.50	1.85	6590.16
	0.480	6570.10	1.85	6570.61
	0.552	6537.70	1.85	6539.83
	0.602	6506.40	1.85	6507.35
	0.650	6465.20	1.85	6464.43
	0.700	6480.10	1.85	6404.61
	0.750	6327.80	1.85	6326.54
	0.800	6227.40	1.85	6227.54
	0.850	6092.60	1.84	6105.30
	0.900	5893.90	1.83	5948.59
	0.965	5322.30	1.79	5638.71
	0.972	4924.30	1.79	5605.31
V	0.225	6262.60	2.11	6262.21
	0.306	6258.00	2.11	6256.90
	0.373	6251.80	2.11	6250.81
	0.472	6240.10	2.11	6237.12
	0.501	6229.60	2.11	6231.18
	0.548	6217.40	2.11	6218.42
	0.596	6198.20	2.11	6199.79
	0.650	6170.90	2.11	6169.48
	0.700	6133.90	2.11	6129.91
	0.750	6083.60	2.11	6076.70
	0.800	6015.50	2.11	6007.43
	0.850	5946.80	2.10	5935.16
	0.900	5859.30	2.09	5838.30
	0.950	5707.50	2.07	5723.14
	1.000	5459.60	2.02	5581.26
	1.030	5132.70	1.99	5454.28
	1.040	4978.20	1.98	5403.50
VI	0.125	5935.30	2.311	5935.36
	0.150	5934.60	2.311	5934.78
	0.200	5933.50	2.311	5933.23
	0.250	5931.70	2.311	5931.14
	0.250	5931.80	2.311	5931.14
	0.300	5929.40	2.311	5928.51
	0.350	5925.50	2.311	5925.25
	0.400	5921.20	2.311	5921.16
	0.450	5914.60	2.311	5915.70
	0.500	5906.40	2.311	5907.86

TABLE I. *(Continued)*

Run	T (K)	$c_{3e}(T)$ (cm/sec)	$D(T)$ (atomic layers)	$c_{3T}(T)$ (cm/sec)	Run	T (K)	$c_{3e}(T)$ (cm/sec)	$D(T)$ (atomic layers)	$c_{3T}(T)$ (cm/sec)
VI	0.525	5899.40	2.311	5902.56	VIII	0.700	4573.60	2.89	4571.07
	0.550	5895.40	2.311	5896.05		0.800	4584.80	2.86	4583.25
	0.575	5887.60	2.311	5888.04		0.900	4651.60	2.77	4667.58
	0.650	5859.90	2.311	5852.08		1.000	4829.70	2.60	4833.07
	0.700	5835.10	2.311	5820.79		1.100	4973.40	2.37	4963.84
	0.740	5810.40	2.310	5803.57		1.190	4479.30	2.11	4774.07
	0.760	5797.80	2.290	5796.05		1.210	4011.40	2.06	4624.20
	0.780	5784.80	2.270	5790.32					
	0.830	5750.90	2.240	5766.73					
	0.860	5730.30	2.210	5742.74	IX	0.200	3656.40	3.31	3656.46
	0.900	5688.80	2.170	5691.80		0.268	3656.00	3.31	3655.94
	0.930	5672.50	2.150	5631.44		0.360	3654.90	3.31	3654.71
	0.950	5647.00	2.110	5577.93		0.465	3652.40	3.31	3652.46
	0.990	5581.70	2.060	5421.21		0.550	3649.30	3.31	3649.87
						0.650	3646.40	3.31	3645.82
						0.800	3690.50	3.27	3688.90
VII	0.109	5109.60	2.49	5110.49					
	0.144	5109.80	2.49	5109.96	X	0.150	2723.25	4.05	2722.59
	0.168	5109.30	2.49	5109.51		0.175	2722.55	4.05	2722.62
	0.207	5108.50	2.49	5108.64		0.200	2720.41	4.05	2722.64
	2.82	5106.10	2.49	5106.46		0.225	2723.05	4.05	2722.66
	0.360	5102.60	2.49	5103.41		0.250	2722.51	4.05	2722.66
	0.445	5096.00	2.49	5098.77		0.300	2720.75	4.05	2722.63
	0.550	5085.20	2.49	5088.79		0.350	2723.95	4.05	2722.56
	0.625	5070.50	2.49	5075.45		0.400	2721.17	4.05	2722.44
	0.700	5054.30	2.49	5053.22		0.450	2722.43	4.05	2722.28
	0.725	5050.70	2.49	5043.22		0.500	2721.42	4.05	2722.10
	0.750	5045.40	2.48	5050.44		0.550	2720.60	4.05	2721.89
	0.800	5047.40	2.46	5058.79		0.600	2720.09	4.05	2721.68
	0.776	5045.40	2.47	5055.12		0.650	2721.16	4.05	2724.01
	0.850	5055.90	2.44	5057.66		0.700	2725.99	4.04	2729.72
	0.900	5084.60	2.40	5079.90		0.750	2738.95	4.02	2748.25
	0.950	5125.10	2.34	5117.68		0.800	2759.67	3.99	2775.57
	1.000	5139.20	2.27	5142.27		0.850	2804.13	3.93	2823.58
	1.060	5146.00	2.15	5147.49		0.900	2864.01	3.86	2886.38
	1.070	5061.60	2.13	5135.63		0.950	2975.67	3.75	2993.38
	1.075	5108.00	2.12	5127.97		0.970	3044.26	3.69	3054.13
	1.100	5044.20	2.07	5069.84		1.000	3146.35	3.58	3160.15
	1.115	4971.40	2.01	5009.68		1.050	3357.62	3.39	3371.12
	1.150	4553.90	1.96	4807.57		1.100	3621.84	3.17	3630.46
	1.160	4165.80	1.94	4723.97		1.150	3921.11	2.92	3959.42
						1.200	4217.98	2.68	4306.81
						1.250	4418.43	2.44	4660.58
VIII	0.178	4611.70	2.89	4611.60		1.271	4448.31	2.36	4767.83
	0.229	4610.90	2.89	4610.89		1.324	4212.90	2.19	4960.15
	0.270	4610.00	2.89	4610.17		1.333	3811.28	2.14	4997.02
	0.300	4609.20	2.89	4609.56					
	0.395	4605.00	2.89	4606.96					
	0.503	4597.20	2.89	4601.73	XI	0.181	1445.80	6.58	1445.97
	0.598	4586.60	2.89	4592.10		0.293	1446.40	6.58	1446.20

TABLE I. *(Continued)*

Run	T (K)	$c_{3e}(T)$ (cm/sec)	$D(T)$ (atomic layers)	$c_{3T}(T)$ (cm/sec)	Run	T (K)	$c_{3e}(T)$ (cm/sec)	$D(T)$ (atomic layers)	$c_{3T}(T)$ (cm/sec)
XI	0.490	1447.40	6.58	1446.19	XI	1.050	1853.40	5.58	1804.35
	0.647	1449.20	6.58	1444.84		1.100	2076.00	5.20	1983.63
	0.700	1452.90	6.55	1453.29		1.150	2481.40	4.69	2271.25
	0.800	1473.80	6.49	1470.20		1.200	2941.40	3.75	2993.01
	0.850	1491.90	6.42	1491.49		1.300	3744.00	3.42	3305.99
	0.900	1533.00	6.32	1523.24		1.350	3904.90	3.14	3606.26
	0.950	1594.90	6.16	1577.16		1.390	3619.80	2.93	3841.84
	1.000	1700.40	5.91	1668.82		1.410	3652.00	2.84	3941.01

flow. We then find the elementary excitation spectrum and calculate the third-sound velocity at finite temperature. The theory is the natural extension to thin films of Landau's bulk superfluid hydrodynamics.[9]

In the discussion of bulk helium or thick helium films one uses the superfluid (particle) density $\rho_s(\vec{r})$ and velocity $\vec{v}_s(\vec{r})$ as well as film thickness as macroscopic variables. As the superfluid surface density falls below a monolayer the thickness clearly fails to describe the coverage. Even for somewhat thicker films it is wrong to model the film as a slab of liquid at bulk density. The only macroscopic variables which one can define are the superfluid surface density $\sigma(\vec{x})$ (atoms per unit area which, at $T=0$, corresponds to $D-a$; see Fig. 5) and the tangential superfluid velocity $\vec{v}_s(\vec{x})$. Here $\vec{x}$ is a two-dimensional vector describing position on the surface.

We now reformulate quantum hydrodynamics using surface quantities. We define a complex order parameter $\psi(\vec{x})$ which is proportional to the wave function of the consensate so that the surface density at $T=0$ of superfluid atoms is

$$\sigma(\vec{x}) = |\psi(\vec{x})|^2 \ . \tag{1a}$$

The usual quantum-mechanical current density is then

$$\vec{j}_s(\vec{x}) = \mathrm{Re}[(\hbar/im)\psi^*\vec{\nabla}\psi] \equiv \sigma(\vec{x})\,\vec{v}_s(\vec{x}) \ , \tag{2}$$

where m is the helium atomic mass. Note that there is no conceptual difficulty in defining a condensate wave function for a two-dimensional system at $T=0$.

There are several terms in the energy of this quantum state. The kinetic energy of the moving film is

$$H_1 = \int d^2x \, \frac{\hbar^2}{2m} |\vec{\nabla}\psi|^2 \ , \tag{3}$$

where the integral is taken over the physical surface area. Since, as argued in Sec. I, the helium atoms propagate in a uniform potential in a liquid with Galilean invariance we will choose m to be the bare ^{4}He mass. The van der Waals binding of the film to the substrate can be represented by the following expression:

$$H_2 = \int d^2x \, \frac{A}{2(a+\sigma)^2} \ , \tag{4}$$

where A and a are constants. The chemical potential term is

$$H_3 = -\int d^2x \, \mu\sigma \ . \tag{5}$$

In addition to these three "obvious" terms, we include a fourth term of the form

$$H_4 = \int d^2x \times \tfrac{1}{2} B(\sigma)(\vec{\nabla}\sigma)^2 \ , \tag{6}$$

where B may be a function of surface density. For thick films we can write $\sigma(\vec{x}) = \rho_0 d(\vec{x})$, where ρ_0 is the bulk particle density and d is the film thickness. Then we have

$$H_4 = \tfrac{1}{2} B(\infty)\rho_0^2 \int d^2x \, (\vec{\nabla} d)^2 \ , \tag{7}$$

which is just the surface energy with $B(\infty)\rho_0^2 = \beta_0$, the surface tension. For bulk helium $\beta_0 = 0.378$ erg cm^{-2}.[19] For thick films H_4 has a simple physical interpretation as a surface energy; for thin films the film thickness and therefore the surface tension are fuzzy concepts and we can only state that a term of this form is permitted by symmetry. The total energy is the sum of these four terms.

To complete the formulation we must write the equation of motion of the condensate wave function. Since ψ is a wave function, the natural equation of motion is the nonlinear Schrödinger equation

$$i\hbar \frac{\partial\psi(x,t)}{\partial t} = \frac{\delta H}{\delta\psi^*(x,t)} \ , \tag{8}$$

where the variational derivative is taken treating ψ and ψ^* as independent quantities. Treating B as a constant, we find

$$i\hbar \frac{\partial\psi}{\partial t} = -\frac{\hbar^2}{2m}\nabla^2\psi - \frac{A\psi}{(a+|\psi|^2)^3} - \mu\psi - B\psi\nabla^2|\psi|^2 \ . \tag{9}$$

One can show easily from this equation that $\sigma(\vec{x})$ obeys the two-dimensional continuity equation

$$\frac{\partial\sigma}{\partial t}+\vec{\nabla}\cdot\vec{j}_s=0\ . \tag{10}$$

This completes the formulation of the theoretical model.

We now examine the solutions of Eq. (9) for the ground state and the low-lying excited states. The ground state is that of the uniform superfluid at rest $\psi(x,t)=\psi_0$. Minimizing the energy with respect to ψ_0 yields

$$\mu=-A/(a+|\psi_0|^2)^3 \tag{11}$$

and a time-independent solution of Eq. (9). The chemical potential is measured relative to the bulk chemical potential. For thick films, $|\psi_0|^2=\rho_0 d$ and the constant A is related to the van der Waals attraction of helium atoms to the argon substrate. We have no measured value for the constant A but Sabisky and Anderson[20] find a theoretical value of $A=14.5$ [K (atomic layers)^3] [we measure σ in atomic-layer units where one atomic layer is $1/(3.6\ \text{Å})^2$]. As the superfluid density goes to zero the chemical potential is $-A/a^3$ which is the chemical potential of the first mobile helium atoms. This form of the chemical potential is valid in the range of 1 to 5 atomic layers as discussed in Sec. I. Our expression, Eq. (4), for H_2 is a phenomenological expression which interpolates smoothly between these limits.

Having found the ground state we look for excited states by examining small phase and amplitude fluctuations of the condensate. That is, we look for collective excitations of the condensate; these excitations are surface density waves which involve motion of the superfluid. We write

$$\psi(x,t)=\psi_0+\gamma(x,t)+i\phi(x,t)\ , \tag{12}$$

where γ is a small amplitude variation of ψ which modulates the surface density and ϕ is a small phase variation of ψ which gives rise to a superfluid velocity. We seek propagating-wave solutions

$$\begin{aligned}\phi(x,t)&=\phi_k\cos(\vec{k}\cdot\vec{x}-\omega_k t)\ ,\\ \gamma(x,t)&=\gamma_k\sin(\vec{k}\cdot\vec{x}-\omega_k t)\ ,\end{aligned} \tag{13}$$

and substitute this expression for $\psi(x,t)$ into the equation of motion, Eq. (9), retaining only first-order terms in γ_k and ϕ_k. We find a solution provided

$$\gamma_k=-(\hbar k^2/2m\omega_k)\phi_k \tag{14}$$

and

$$(\hbar\omega_k)^2=\frac{3A\sigma_0\hbar^2k^2}{m(a+\sigma_0)^4}+(\hbar^2k^2/2m)^2(1+4Bm\sigma_0/\hbar^2)\ , \tag{15}$$

where $\sigma_0=|\psi_0|^2$ is the average superfluid surface density of the film. The frequencies given by Eq. (15) are the frequencies of the collective modes of the condensate which are the elementary excitations of the thin film. These elementary excitations are surface density waves with a linear dispersion and a sound velocity $c^2=3A\sigma_0/m(a+\sigma_0)^4$ at long wavelengths and an upward dispersion for shorter wavelengths. We call these elementary excitations surface phonons. In the thin film limit the elementary excitation spectrum approaches the free particle energy for large k.

Note that a collective mode of any amplitude is a valid solution of Eq. (9); the amplitude is not quantized. This emphasizes that we have treated the equation of motion (9) as a classical field equation and $\psi(x,t)$ as a classical field. This is perfectly valid in treating a condensate wave function since quantum fluctuations of the wave function amplitude are unimportant. At this point, however, we wish to compute thermodynamic quantities and we must quantize the theroy. We neglect the interactions among the elementary excitations and the Hamiltonian is simply the sum of harmonic oscillators with frequencies ω_k. We compute thermodynamic quantities from the elementary excitation spectrum in the usual way.[21]

The theory is based on macroscopic quantum hydrodynamics and the elementary excitation spectrum equation (15) is expected to be valid only for wave numbers less than 1 per interparticle spacing and less than 1 per superfluid film thickness. For short wavelengths and thicker films we expect our surface-wave excitation to go over smoothly to the classical ripplon excitation[4] We can easily modify our dispersion relation so that it goes over to this limit correctly:

$$\begin{aligned}(\hbar\omega_k)^2=\Bigg[&\frac{3A\sigma_0\hbar^2k^2}{m(a+\sigma_0)^4}+\left(\frac{\hbar^2k^2}{2m}\right)^2\\ &\times\left(1+\frac{4Bm\sigma_0}{\hbar^2}\right)\Bigg]\tanh\left(\frac{k\sigma_0}{\rho_0}\right)\Bigg/\left(\frac{k\sigma_0}{\rho_0}\right)\ .\end{aligned} \tag{16}$$

This correction is not very important for the range of film thicknesses and temperatures where the surface phonons are the dominant excitations.

We observe in our experiment an excitation which is consistent with a "surface-roton" model with an energy gap. This is presumably closely related to the two-dimensional roton studied theoretically by Padmore using the Feynman-Cohen method.[11] A simple intuitive picture of this excitation is that of a bound pair of vortices of opposite circulation, with the surface roton being the smallest or most tightly bound pair permitted by quantum mechanics. We will assume a phenomenological dispersion relation in the surface-roton region

$$\hbar\omega_k = \Delta + \hbar^2(k-k_0)^2/2m^* \tag{17}$$

in close analogy to the bulk-roton dispersion relation. The two branches of the dispersion curve cross at a wave number k_c. The thermodynamics is insensitive to the details of this crossover region; we retain the surface-phonon branch for $k < k_c$ and the surface-roton branch for $k > k_c$.

B. Third-sound velocity

At finite temperature the third-sound wave is a long-wavelength surface density wave accompanied by a temperature wave. The thermally excited elementary excitations behave as a "normal fluid" which is pinned to the substrate. The superfluid surface density $\sigma_s(T)$ can be calculated using an argument due to Landau. The thermodynamic energy $E(\sigma_0,T)$ is a well defined function of surface density σ_0 and temperature. The work done to increase the surface density by an amount $d\sigma_0$ is

$$dW = \left(\frac{dE}{d\sigma_0}\right)_S d\sigma_0 \ . \tag{18}$$

Now using the standard macroscopic hydrodynamic argument, the third-sound velocity under adiabatic conditions is

$$c_3^2(T) = |K(T)\sigma_s(T)/m| \ , \tag{19}$$

where the adiabatic elastic constant is

$$K(T) \equiv \left(\frac{d^2E}{d\sigma_0^2}\right)_S \ . \tag{20}$$

This assumes that the thermal boundary resistance between the substrate and the elementary excitations in the film is large enough that the thermal equilibration time is much longer than the period of the third-sound wave; this condition is satisfied at low temperatures in the present experiment. One can define an isothermal third sound velocity but we will not need this quantity.

The thermally excited elementary excitations affect the third-sound velocity in two ways. First, as discussed above, the superfluid surface density is reduced at finite temperature. Second, the energy of the elementary excitations is a function of surface density, so that the elementary excitations also modify the elastic constant. We now calculate these two effects.

The free energy per unit area is

$$F(\sigma_0,T) = \frac{\frac{1}{2}A}{(a+\sigma_0)^2} + T\sum_k \ln(1-e^{-\epsilon_k/T}) \ , \tag{21}$$

where $E(k) = \hbar\omega_k$ is the elementary-excitation energy. Since $dW = \mu\, d\sigma_0$, we have

$$\mu = \left(\frac{dF}{d\sigma_0}\right)_T = \left(\frac{dE}{d\sigma_0}\right)_S \tag{22a}$$

and

$$K(T) = \left(\frac{d\mu}{d\sigma_0}\right)_S = \left(\frac{\partial\mu}{\partial\sigma_0}\right)_T - \left(\frac{\partial\mu}{\partial T}\right)_{\sigma_0} \times \left(\frac{\partial S}{\partial\sigma_0}\right)_T \Bigg/ \left(\frac{\partial S}{\partial T}\right)_{\sigma_0} \ , \tag{22b}$$

with

$$S = -\frac{\partial F}{\partial T} \ . \tag{22c}$$

where μ, S, and F are considered to be functions of σ_0 and T, and $E(k)$ is a function of σ_0. The differentiations in Eq. (22) can be carried out analytically and the sum over k performed numerically to find $K(T)$. At low temperature we can approximate the elementary excitation spectrum by $E(k) \simeq \hbar kc$ and carry out the integration analytically to find

$$K(T) \simeq \frac{3A}{(a+\sigma_0)^4} + \frac{1.202T^3}{\pi\hbar^2c^3}\frac{\partial^2 c}{\partial\sigma_0^2} \ . \tag{23}$$

In order to find the superfluid surface density we follow Landau and calculate the momentum of the moving fluid with the elementary excitations at equilibrium in the rest frame

$$\vec{\mathrm{P}} = m\sigma_0\vec{\mathrm{v}}_s + \sum_k \hbar\vec{\mathrm{k}}n_k \equiv m\sigma_s(T)\,\vec{\mathrm{v}}_s \ , \tag{24}$$

where the number of excitations of momentum k is

$$n_k = \frac{1}{\exp\{[E(k)+\hbar\vec{\mathrm{k}}\cdot\vec{\mathrm{v}}_s]/T\}-1} \ . \tag{25}$$

We find

$$\sigma_s(T) = \sigma_0 - \sum_k \frac{\hbar^2k^2}{2mT}\frac{e^{E(k)/T}}{(e^{E(k)/T}-1)^2} \ . \tag{26}$$

The integral can be performed numerically for the general case; at low temperature we find

$$\sigma_s(T) \simeq \sigma_0 - 3\times 1.202T^3/2\pi m\hbar^2c^4 \ . \tag{27}$$

We see that the third-sound velocity approaches the surface-phonon velocity at low temperature with corrections proportional to T^3:

$$c_3^2(T) \simeq c^2\left[1 - \frac{1.202T^3}{2\pi m\hbar^2c^4\sigma_0} \times \left(\frac{3}{2} - \frac{\sigma_0^2}{c}\frac{\partial^2 c}{\partial\sigma_0^2}\right)\right] \ . \tag{28}$$

At higher temperature there are deviations from the T^3 law due to dispersion and the integrals in Eq. (21) and (26) must be performed numerically. It is convenient to write

$$c_3^2(T) = c^2[1 - \alpha(T)T^3] \ , \tag{29}$$

and to discuss the quantity $\alpha(T)$. At low temperature only the linear portion of the excitation spectrum is involved and $\alpha(T)$ is a constant. At intermediate temperatures the upward dispersion of the excitation spectrum is important in reducing the number of excitations and $\alpha(T)$ decreases. Finally, at high temperature (0.6 K) the surface roton branch is excited and $\alpha(T)$ increases exponentially.

We make two approximations in the numerical work which are numerically unimportant. In the calculation of $K(T)$ we neglect $dB/d\sigma_0$ and $d\Delta/d\sigma_0$. It turns out that $d\Delta/d\sigma_0$ is small over most of the range of film thicknesses studied. For small coverage corrections to the velocity enter as $(d\Delta/d\sigma_0)^2$ and could be included. The result would be a reduction in the magnitude of $d\Delta/d\sigma$ and a further flattening of the curve in Fig. 9. We have not done this since the errors due to the model and experiment both become large for $a < 2$ atomic layers. Thus the entire surface roton correction appears in $\sigma_s(T)$. We do not correct for the transition from adiabatic to isothermal behavior at high temperature; the surface rotons are the dominant excitation in this temperature range and the surface-roton corrections to $K(T)$ has already been neglected.

IV. ANALYSIS OF DATA

For small k, $E(k)$ is given by Eq. (16) and requires three parameters: σ_0, μ, and B. For large k, $E(k)$ is given by Eq. (17) and also requires three parameters: Δ, k_0, and m^*. With $E(k)$ given in these two domains, $\sigma_s(T)$ and $K(T)$ are generated numerically via Eqs. (26) and (22) and then $c_3(T)$ is calculated and compared with the experimental results as shown in Fig. 3.

Because of the dominant T^3 behavior, comparison is also made with the function

$$\alpha(T) = \frac{1 - c_3^2(T)/c^2}{T^3} \ , \tag{30}$$

as shown in Fig. 4. In fact the experimental curve $\alpha(T)$ motivated the attempt to make detailed calculations of $E(k)$ for thin films. The remarkable precision of our measurement allows us to measure the deviations of $E(k)$ from a linear dispersion. If only dispersionless, surface phonons were present and $\partial c/\partial\sigma_0$ were zero then $\alpha(T)$ would be independent of temperature. Had the scatter in the measurements of the third sound velocity below 0.6 K been as large as 1 part in 10^3, the experimental $\alpha(T)$ would have been scattered about a horizontal line and $E = \hbar ck$ would have been consistent with our measurements.

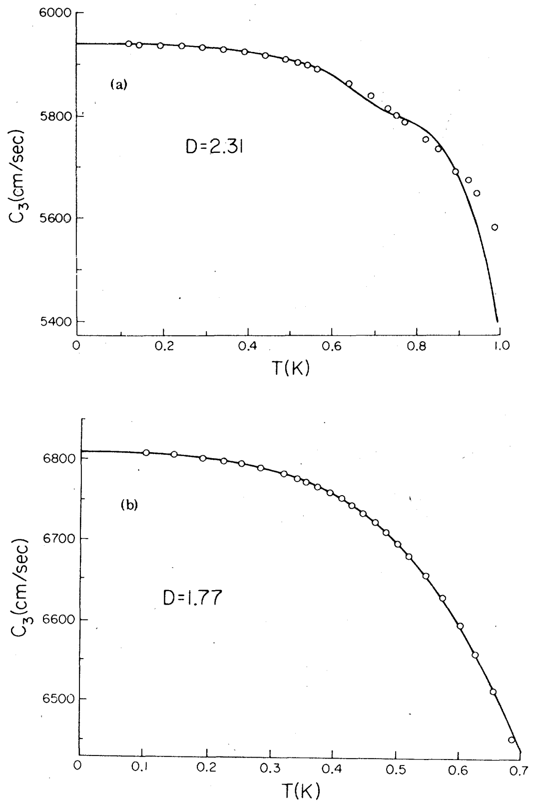

FIG. 3. Open circles are the measurements of third-sound velcoity vs temperature. At low temperatures the resolution is 2 parts in 10^5; note the expanded scale on the ordinate. The solid line is our model of two-dimensional superfluidity discussed here. D is the coverage of ^{4}He in atomic layers.

Since the net coverage D is determined from the vapor-pressure measurements, there are only two independent parameters needed for small k since

$$D = a + \sigma_0 . \tag{31}$$

However, we can also determine a directly from the third-sound data. Since measured values of $c_3(T)$ are within 1% of c we can, for this analysis, let c equal the coldest measured value of the third-sound velocity. At $T = 0$, Eqs. (23) and (27) can be substituted into Eq. (19) using Eq. (31) to give

$$c^2D^4 = (3A/m)(D - a) \ . \tag{32}$$

In Fig. 5 the intercept gives a value for a of 1.25 ± 0.05 atomic layers. a is considered as that portion of the ^{4}He coverage which does not participate in third-sound wave motion. No more can be said about a. We cannot tell whether a is the coverage of frozen helium or of some temperature-independent normal fluid, or a combination of both. From the slope of the line drawn in Fig. 5, A is 13.7 K which is within 6% of

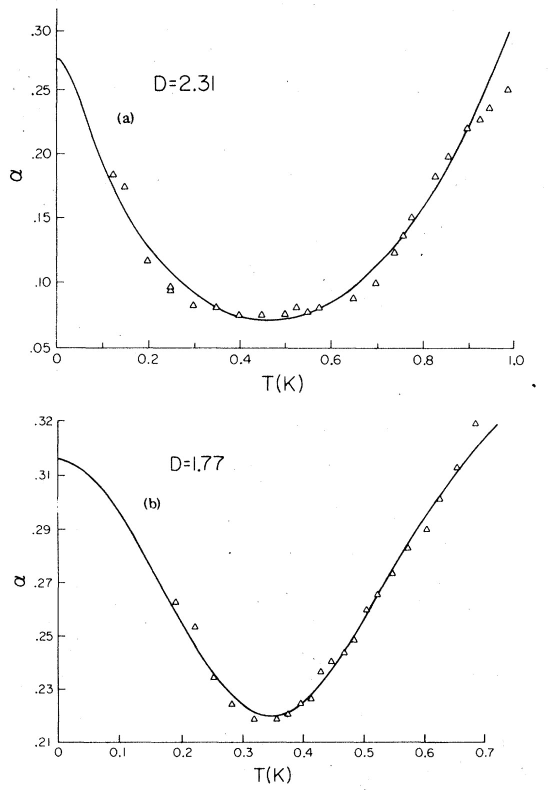

FIG. 4. Open triangles are from experiment and the solid line from the theory discussed here. α is defined by Eq. (30) and would be independent of temperature if dispersionless two-dimensional phonons were the only excitations. At low temperatures the downward trend is due to surface tension; at higher temperatures the upward trend is due to surface-roton excitations.

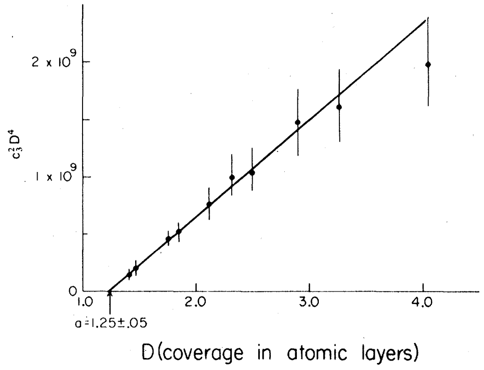

FIG. 5. Tests of the validity of Eq. (32) near $T=0$ and the intercept gives $a = 1.25 \pm 0.05$ atomic layers. a is the coverage of ^{4}He which does not participate in third-sound wave motion. The vertical error bars result from an uncertainty of the coverage of $\pm 5\%$. That the slope is within 6% of 14.5 K indicates that the geometric path length chosen for the third-sound resonance ($L = 3.82$ cm) is within 3% of the actual path length.

the calculated value for an argon substrate of 14.5 K. In practice then there is only one adjustable parameter for T less than about 0.4 K, the surface tension. However, c becomes our second working parameter for low k because D and a are known to only a few percent and c must be adjusted to a part in 10^5 for the analysis of the surface tension. Of the three adjustable parameters for high k, the effective mass m^*, and the momentum of the roton minimum k_0 can be combined into a single parameter $(m^* k_0^6)$. Since we cannot separate m^* from k_0 in this analysis we have arbitrarily fixed m^* to $0.2m$, the value of the roton

TABLE II. Results of fitting theory to experiment. c is the surface phonon velocity for $k=0$ and the third-sound velocity for $T=0$. B is the surface energy in the thick-film limit. Δ is the energy of the roton minimum and k_0 is the momentum of the roton minimum.

Run	$D(0)$ (cm) ($\pm 5\%$)	c (cm/sec) (± 0.1)	B (erg/cm^2) (± 0.025)	Δ (K) (± 0.2)	k_0 (Å^{-1}) (± 0.1)
I	1.41	6340.0	0.05	2.40	0.8 ± 0.5
II	1.45	6281.3	0.02	3.15	1.35 ± 0.1
III	1.77	6807.2	0.12	3.35	0.9
IV	1.85	6622.1	0.27	4.90	1.6
V	2.11	6267.2	0.23	5.26	1.9
VI	2.35	5936.4	0.30	5.22	2.0
VII	2.49	5111.2	0.34	5.40	1.8
VIII	2.89	4612.8	0.32	5.32	1.8
IX	3.31	3657.1	0.33	$8.4 \pm .5$	1.85
X	4.05	2722.5	0.37	$8.0 \pm .5$	1.8
XI	6.58	1445.8	0.37	8.0 ± 1	1.9 ± 0.2

effective mass for bulk helium. A partial justification for this choice is the resulting behavior of k_0 as a function of coverage. To leave k_0 fixed and vary m^* during the fitting procedure would have produced unphysically small values for m^* of $10^{-3}m$.

Evaporation of the thicker films above 0.7 K produces significant changes of the adjustable parameters. Since the thinner films were studied first, these changes were incorporated in the thicker-film analysis. To adjust c we use the expression based on Eq. (32),

$$c(D(T)) = c\frac{[D(T)-a]^{1/2}D^2(0)}{[D(0)-a]^{1/2}D^2(T)} . \tag{33}$$

This is the most important thickness correction.

To adjust B, we use

$$B(D(T)) = 0.378\frac{[D(T)-a]^3}{d_c^3+[D(T)-a]^3} . \tag{34}$$

This function has no physical basis but provides an adequate description of the surface tension for thinner films. d_c is found to be 0.6 atomic layers. These two corrections provided more than a tenfold reduction in χ^2 for the thicker films. Similar corrections for Δ and k_0 were tried and found to make no significant improvement in the fitting and thus were not used.

Fitting was carried out by displaying the experimental $c_3(T)$ and $\alpha(T)$ on a graphic display terminal. Fitting parameters were inputed and the computer generated numerically a $c_3(T)$ and $\alpha(T)$ and superimposed these curves on the experimental curves. The value of χ^2 for the fit was also displayed. In this fashion not only χ^2 could be minimized but slopes and curvatures could quickly be matched. In practice fitting with the four working parameters c, B, Δ, and k_0, using $\alpha(T)$, breaks down into two rather-rapid two-parameter fits. Below 0.4 K, c and B are important. Adjusting c brings $\alpha(T)$ for theory and experiment together and adjusting B matches the slopes of the $\alpha(T)$'s. At higher temperatures, Δ and k_0 dominate. Adjusting the numeric ratio Δ/k_0 brings $\alpha(T)$ for theory and experiment together and adjusting k_0 matches the high-temperature curvature of $\alpha(T)$.

There are at least three limitations of this analysis. First, for the thinnest film studied the roton and surface-phonon portions of $E(k)$ have moved so closely together as to make a separate description of them questionable. The details of the intermediate region of k are important only for the two thinnest films and will modify both B and k_0. Second, at about 0.6 K the surface phonons are more correctly described as isothermal, wehreas we have used the adiabatic form of $K(T)$. In most cases the roton contributions to $\alpha(T)$ have, at the same temperatures, become large enough to swamp this difference. This difficulty can be seen in Fig. 4(a) where, at intermediate temperatures the data is flatter than the theory. Finally, for the thickest two films reported here, 4.05 and 6.58 atomic layers, accurate analysis becomes impossible because of a rapidly changing film thickness. In fact, for such thick films, the two-dimensional model developed in Sec. II is probably no longer valid.

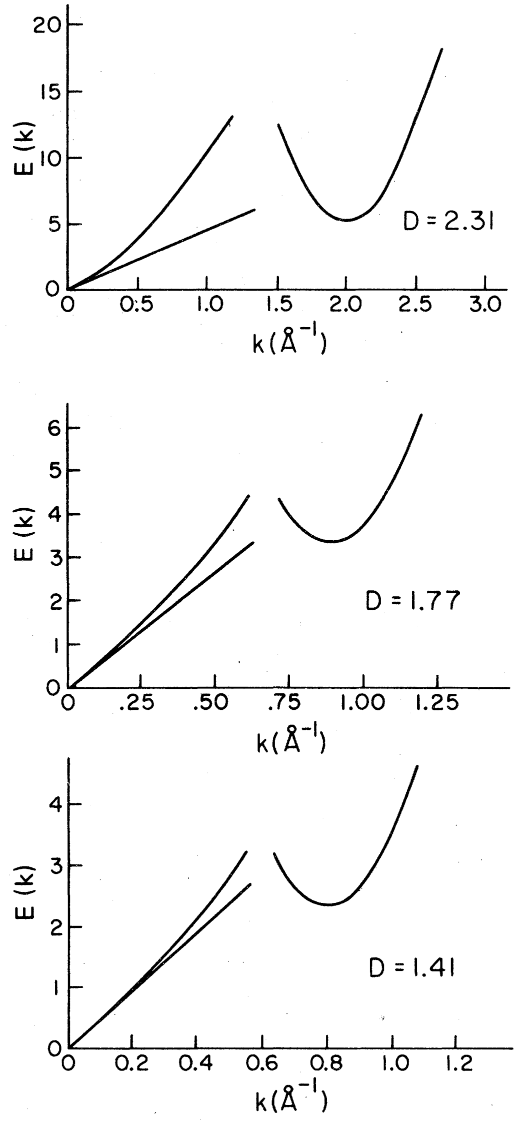

FIG. 6. $E(k)$ for three coverages of ^{4}He based on a fit of theory to experiment. There is no component of k perpendicular to the film. Near $k=0$ the slope approaches the $T=0$ third-sound velocity indicated by the straight line. For larger k the surface energy causes an upward bending which is larger for thicker films. For large k a surface-roton contribution is required to describe the experimental results. The crossover region between surface phonons and surface rotons has not been drawn because neither theory nor experiment describe this region.

V. CONCLUSIONS

Table II summarizes the results of fitting theory to experiment. The errors represent the range over which a good fit can be made while optimizing the other parameters. In Fig. 6 the resulting $E(k)$ is plotted for three thicknesses. The intermediate range of $E(k)$ is not shown since we have no information or model to reveal this region.

Perhaps the most satisfying result is in the thick-film limit where surface tension, energy gap, and roton minimum approach the bulk values as indicated by the arrows in Figs. 7–9 (the thickest film is not shown in these figures but appears in Table II). There was no *a priori* reason, within the theory, for this to happen.

The straight line in Fig. 6 has a slope of c for each film thickness. The rise of the surface phonon branch above this line illustrates the effect of the free particlelike excitations for very thin films and in addition, ripplons for thicker films. As shown in Fig. 7 when D approaches a, the superfluid surface tension falls to zero. The curve drawn through the points in Fig. 7 has the functional form given by Eq. (34) with a characteristic thickness of 0.6 atomic layers.

Both the roton gap and roton minimum fall toward zero along with the surface tension. Again, they both turn downward in the vicinity of a as shown in Figs. 8 and 9. Both the reduction in surface tension and the reduction in k_0 indicate a decrease in the surface density of the mobile portion of the film. The energy gap behaves in a rather peculiar fashion, having a constant value of 5.3 ± 0.1 K between a D of two and three atomic layers. Finally, for larger D the gap abruptly jumps to near its bulk value.

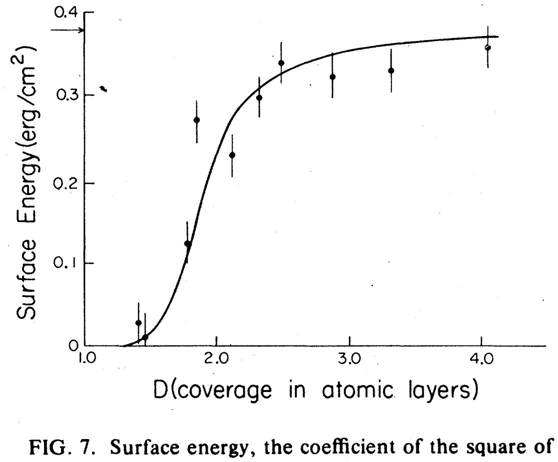

FIG. 7. Surface energy, the coefficient of the square of the gradient of the coverage, required to fit experiment. The arrow at the top of the ordinate indicates the surface energy of bulk ^{4}He. The surface energy is near zero while the film is still superfluid indicating a two-dimensional gaslike state.

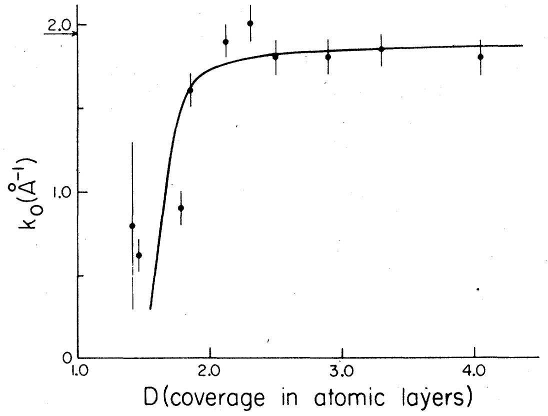

FIG. 8. Momentum of the roton minimum k_0 required to fit experiment. The arrow at the top of the ordinate indicates the value of k_0 for bulk ^{4}He. The fall of k_0 with smaller D indicates, as does surface tension, that the superfluid is becoming more gaslike as D approaches a.

We have presented high-precision measurements of third-sound velocity versus temperature for several very thin films. We have developed a quantum-hydrodynamic theory of the elementary excitation spectrum at long wavelength and have calculated the third-sound velocity. The theory permits a quantitative interpretation of our data in terms of an elementary excitation spectrum and we have determined an elementary excitation spectrum for superfluid surface densities from 0.16 monolayer to 5.25 monolayers.

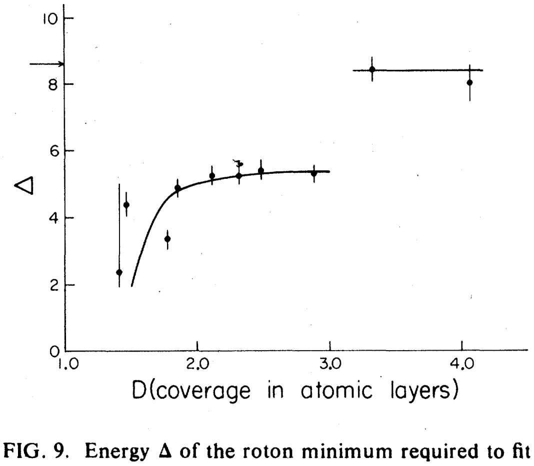

FIG. 9. Energy Δ of the roton minimum required to fit experiment. The arrow at the top of the ordinate indicates the value of Δ for bulk ^{4}He. The average value of Δ between 2 and 3 atomic layers is 5.3 ± 0.1 K. The sharp jump to the bulk value of Δ is not understood.

The fact that the experimental $\alpha(T)$ curves go through a minimum shows that the real dispersion curve must bend upward for small k and then bend down again for larger k. We have forced our theoretical dispersion to bend properly by replacing the surface-phonon branch by a surface-roton branch for $k > k_c$ and rather arbitrarily assumed that the roton effective mass was the same as that for bulk rotons. The details of our dispersion curve may not be right in that the region around k_c may not be as sharply peaked and the roton minimum may be shallower than the dispersion curves shown in this paper, especially in the thinner films. The surface tension, roton gap, and roton momentum from the fitting all go to their proper bulk helium values as the film thickens. As the surface density falls toward a, the surface energy and the roton minimum move toward zero. In this respect, the films begin to resemble two-dimensional superfluid gas. Thus we have shown that the third-sound measurements provide a detailed, quantitative probe of the elementary excitation spectrum in thin superfluid-helium films.

---

[*] Work supported by the NSF under Grants Nos. NSF-DMR-72-03291 and NSF-DMR-76-01058.

[1] C. W. F. Everitt, K. R. Atkins, and A. Denenstein, Phys. Rev. Lett. 8, 161 (1962).

[2] K. R. Atkins, Physica (Utr.) 23, 1143 (1957); Phys. Rev. 113, 962 (1959).

[3] C. H. Anderson and E. S. Sabisky, Phys. Rev. Lett. 24, 1049 (1970).

[4] C. G. Kuper, Physica (Utr.) 22, 1291 (1956); 24, 1009 (1956).

[5] R. S. Kagiwada, J. C. Fraser, I. Rudnick, and D. Bergmann, Phys. Rev. Lett. 22, 338 (1969).

[6] J. H. Scholtz, E. O. McLean, and I. Rudnick, Phys. Rev. Lett. 32, 147 (1974).

[7] V. L. Ginzburg and L. P. Pitaevskii, Sov. Phys.-JETP 7, 858 (1958).

[8] T. E. Washburn, J. E. Rutledge, and J. M. Mochel, Phys. Rev. Lett. 34, 183 (1975).

[9] L. Landau, J. Phys. (USSR) 5, 71 (1941).

[10] T. C. Padmore and J. D. Reppy, Phys. Rev. Lett. 33, 1410 (1974).

[11] T. C. Padmore, Phys. Rev. Lett. 32, 826 (1974).

[12] M. Chester and L. Eytel, Phys. Rev. B 13, 1069 (1976).

[13] J. E. Berthold, D. J. Bishop, and J. D. Reppy (unpublished).

[14] E. Lerner and J. G. Daunt, J. Low Temp. Phys. 10, 299 (1973).

[15] "DAG" No. 154, Acheson Colloids, Co., Port Huron, Mich.

[16] National Bureau of Standards superconducting fixed points, Model SRM 767, Serial No. 86.

[17] Cryo Cal, Inc., Model CR1000, Serial No. 4692.

[18] A. C. Anderson, Rev. Sci. Instrum. 44, 1475 (1973).

[19] D. O. Edwards, P. P. Fatouros, G. G. Ihas, P. Mrozinski, and S. Y. Shen, Phys. Rev. B 11, 4734 (1975).

[20] E. S. Sabisky and C. H. Anderson, Phys. Rev. A 7, 790 (1973).

[21] L. D. Landau and E. M. Lifshitz, *Statistical Physics*, Vol. 5 of Course of Theoretical Physics, 2nd ed. (Addison-Wesley, Reading, Mass., 1970).